Predictions of ion energy distributions and radical fluxes in radio frequency biased inductively coupled plasma etching reactors

Robert J. Hoekstra[a] and Mark J. Kushner[b]
Department of Electrical and Computer Engineering, University of Illinois, Urbana, Illinois 61801

(Received 23 August 1995; accepted for publication 20 November 1995)

Inductively coupled plasma (ICP) reactors are being developed for low gas pressure (<10s mTorr) and high plasma density ($[e]>10^{11}$ cm^{-3}) microelectronics fabrication. In these reactors, the plasma is generated by the inductively coupled electric field while an additional radio frequency (rf) bias is applied to the substrate. One of the goals of these systems is to independently control the magnitude of the ion flux by the inductively coupled power deposition, and the acceleration of ions into the substrate by the rf bias. In high plasma density reactors the width of the sheath above the wafer may be sufficiently thin that ions are able to traverse it in approximately 1 rf cycle, even at 13.56 MHz. As a consequence, the ion energy distribution (IED) may have a shape typically associated with lower frequency operation in conventional reactive ion etching tools. In this paper, we present results from a computer model for the IED incident on the wafer in ICP etching reactors. We find that in the parameter space of interest, the shape of the IED depends both on the amplitude of the rf bias and on the ICP power. The former quantity determines the average energy of the IED. The latter quantity controls the width of the sheath, the transit time of ions across the sheath and hence the width of the IED. In general, high ICP powers (thinner sheaths) produce wider IEDs.
© *1996 American Institute of Physics.* [S0021-8979(96)02905-3]

I. INTRODUCTION

Inductively coupled plasmas (ICP) are being investigated for use as sources for etching of dielectrics and metals for semiconductor microelectronics fabrication.[1–9] ICP reactors typically operate at low gas pressures (<10–20 mTorr) and high plasma densities (10^{11}–10^{12} cm^{-3}). The plasma is generated by either a solenoidal or flat spiral coil operated at hundreds kHz to tens of MHz. A separate radio frequency (rf) bias (a few MHz to tens of MHz) is applied to the substrate to accelerate ions anisotropically into the wafer that is being processed. A feature of this type of reactor is that the magnitude of the ion flux and ion energies incident onto the wafer can, in principle, be separately controlled. The former is determined by the inductively coupled power from the coil. The latter is controlled by the amplitude of the rf bias applied to the substrate.

Measurements of the plasma properties of ICP reactors have, to date, concentrated on optical emission and electric probe measurements of electron densities and electron energy distributions. Of these studies, few have investigated ion properties. O'Neill *et al.*[5] measured optical emission from argon ions in ICP reactors and showed that the ion temperature was ≤0.5 eV at pressures <10–20 mTorr. Hopwood[10] and Kortshagen[11] measured the ion energy distribution (IED) of Ar ions striking a grounded substrate in ICP reactors without an applied bias. They found that the width of the IED was a few eV. Hopwood attributed a portion of this width to rf variation in the plasma potential presumably due to stray capacitive coupling. In the absence of this capacitive coupling, the broad distributions may be explained by ion acceleration in a mildly collisional presheath, or ion production over a large range of plasma potentials. Zheng *et al.* have shown that etching profiles of polysilicon (p-Si) in inductively coupled plasmas are best explained by having ions enter the sheath from the presheath with ≈0.5 eV temperature.[12] When a capacitive rf bias is applied to the substrate, or there is capacitive coupling from the coils, the plasma potential will be modulated. As a result, the width of the IED will broaden as in conventional reactive ion etching (RIE) discharges. This broadening was demonstrated by Caughman.[13]

It is a well-known phenomenon that in RIE discharges that the shape of the IED is a function of the ion transit time across the sheath.[14–19] If the ion transit time is short compared to the rf period, the ion experiences the instantaneous sheath potential. The resulting IED then has a double peak appearance attributed to ions entering the sheath when its potential is at the low and high energy extremes. If the ion transit time is long compared to the rf period, the ion experiences only the time averaged sheath potential, and the IED has a single peak. A convenient scaling parameter is[15]

$$S=\frac{\tau_t}{\tau_{\rm rf}}=\left(\frac{2M\lambda^2}{qV}\right)^{1/2}\nu_{\rm rf}, \qquad (1)$$

where τ_t is the transit time of the ion, $\tau_{\rm rf}$ is the rf period, λ is the sheath thickness, M is the ion mass, V is the rf potential amplitude, and $\nu_{\rm rf}$ is the rf frequency. If $S\gg1$, the IED will be single peaked. If $S\ll1$, the IED will be double peaked.

In an ICP etching reactor the plasma density is typically larger (≥10^{11} cm^{-3}) than that found in conventional RIE discharges (10^9–10^{10} cm^{-3}). Since the rf sheath thickness scales inversely with plasma density, λ is typically small in these reactors, ≤1 mm. As a result, the sheath velocity is small and stochastic heating of electrons is minimal. The end result is that the electron density $[e]$ is largely a function of

[a]Electronic mail: stretch@uigela.ece.uiuc.edu
[b]Electronic mail: mjk@uiuc.edu

inductively coupled power, P, and in most cases is a weak function of the rf bias. Experimental and theoretical results have shown that $[e]$ is nearly linearly proportional to P in a variety of gases.[9,20,21] Since the IED shape parameter S is a function of λ, which in turn depends upon $[e]$, one can expect that the shape of the IED will be a function of inductively coupled power. Although $[e]$ and the average ion power density can, to first order, be independently controlled by the inductively coupled power and rf bias, these two quantities are ultimately coupled through the dependence of the IED on the sheath width.

To illustrate this dependence, we can estimate the amplitude of the rf sheath width by[22]

$$\lambda = \frac{j}{q 2\pi \nu_{\mathrm{rf}}[e]} \approx \frac{j}{q 2\pi \nu_{\mathrm{rf}} a P}, \tag{2}$$

where j is the rf current density and we have assumed that $[e]=aP$. The shape parameter for the IED is then

$$S = \frac{j}{q 2\pi a P}\left(\frac{2M}{qV}\right)^{1/2}. \tag{3}$$

At large inductively coupled powers, and hence large electron densities, S is small. The IED should then be broad. At small inductively coupled powers, S is large and the IED should be narrow.

In this article, we describe a model for IEDs onto the wafer as a function of radius in inductively coupled plasma reactors for etching. The model is a two-dimensional plasma chemistry Monte Carlo simulation (PCMCS) which tracks the trajectory of pseudoparticles representing ions and radicals as a function of phase during the rf cycle. The PCMCS accepts electric fields and electron impact source functions for these species from a companion hybrid plasma equipment model (HPEM). We found the width (in energy) of the IED is a sensitive function of ICP power deposition in the critical region which produces plasma densities from low 10^{10} to high 10^{11} cm^{-3}. Higher power deposition generating a larger plasma density and thinner sheaths produces broader IEDs. The IEDs are, though, generally uniform as a function of radius across the wafer. Some, systematic thinning of the width of the IED at large radii can be attributed to decreases in plasma density near the edge of the wafer. We also predict etching rates for poly-Si using the mechanism proposed by Dane and Mantei.[23] We found that in the parameter space of interest (ICP powers of hundreds of W, rf bias voltages of 50–150 V), etching is typically in the ion starved regime. Etch uniformity is therefore determined by the ion flux uniformity.

Our model will be described in Sec. II, followed by a discussion of our results for IEDs in Sec. III and for etching rates in Sec. IV. Our concluding remarks are in Sec. V.

II. DESCRIPTION OF THE MODEL

The computer model we have used in this study consists of two linked simulations. The first is called the hybrid plasma equipment model (HPEM).[20] The HPEM is a model of the electromagnetic field, electron kinetics, and plasma chemistry in a plasma etching reactor. The HPEM treats electron transport kinetically using a Monte Carlo simulation. Heavy particle transport, however, is treated using fluid equations. As a consequence kinetic information such as energy distribution functions is not generated. To obtain these quantities, the electric fields and electron impact source functions for heavy particles generated by the HPEM are used in the second simulation called the plasma chemistry Monte Carlo simulation (PCMCS). The PCMCS tracks the trajectories of all neutral and charged heavy particles as a function of position and phase during the rf cycle, producing densities, fluxes, and energy distributions. The HPEM has been previously described,[20] and so will be only briefly discussed here. The PCMCS will be discussed in detail.

A. HPEM

The two-dimensional HPEM is composed of a series of modules which are iterated to a converged solution. The electromagnetics module (EM) calculates inductively coupled electric and magnetic fields in the reactor. These fields are next used in the electron Monte Carlo simulation (EMCS) module. In the EMCS electron trajectories are followed for many rf cycles producing the electron energy distribution as a function of position and phase. These distributions are used to produce electron impact source functions which are transferred to the fluid kinetics simulation module (FKS). In the FKS, continuity and momentum equations are solved for all neutral and heavy charged species, and Poisson's equation is solved for the electric potential. The FKS also imports an externally generated advective flow field produced in a hydrodynamic module (HM). The HM is a solution of the fully compressible fluid conservation equations for continuity, momentum, and energy. Slip boundary conditions are used to extend the fluid equations to the low pressure ranges of interest (5–20 mTorr). The plasma conductivity produced in the FKS is passed to the EM, and the species densities and time dependent electrostatic potential are passed to the EMCS. The modules are iterated until cycle averaged plasma densities converge. Acceleration algorithms are used to speed the rate of convergence of the model.

In an improvement to the previously described model, we have implemented a semianalytic sheath model in the HPEM. The purpose of this improvement is to address conditions where the mesh spacing Δx exceeds the actual sheath thickness at boundaries. If the mesh is too coarse to resolve the sheath, the apparent sheath thickness is that of the mesh spacing adjacent to the surface. The sheath voltage is then dropped across the width of the numerical cell. For low pressures where the sheath is collisionless, the sheath voltage and other parameters are little affected by the artificially large sheath thickness. However, in not resolving the sheath, the electric field in the sheath is diminished by the ratio of $\lambda/\Delta x$.

There have been a number of works in which semianalytic models have been proposed for rf discharges which make different approximations.[22,24,25] For example, the model presented by Lieberman[22] assumes the ions respond to the time averaged sheath potential while that of Metze *et al.*[25] assume the ions respond to the instantaneous sheath potential. Our parameter space is likely between those two

extremes. In experiments by Manenschijn *et al.*,[24] the IEDs striking the powered electrode in an RIE reactor were measured. They found that at low pressures where ion transport is collisionless (<5 mTorr) the optical sheath thickness was well represented by the collisionless Child–Langmuir relationships. For the same conditions, the Lieberman model[22] would provide a thicker sheath due to the presence of electrons in the sheath. The choice of which sheath model to use in this work was influenced by two factors. The first is that few of the previously published models have been applied and validated in the parameter space of interest. The second is that since the sheath model will be applied at every boundary point in the two-dimensional mesh, a relatively straightforward model is required which will execute rapidly.

In our semianalytic model, we obtain the sheath thickness in the following fashion. We separately compute the conduction and displacement current to each location on the two-dimensional plasma-material boundary in the HPEM. The displacement current obtained using the mesh limited sheath thickness Δx is j_{d0}. With knowledge of the plasma density adjacent to the sheath $[e]$, we can compute the expected rf amplitude of the oscillating sheath thickness assuming a capacitive ion matrix sheath λ:

$$\lambda = \frac{j_d}{2\pi\nu_{\rm rf}\, q[e]}, \tag{4}$$

where j_d is the actual displacement current density. The ratio of the actual sheath thickness to the mesh spacing is then

$$\frac{\lambda}{\Delta x} = \frac{j_{d0}}{j_d} = \frac{j_{d0}}{\lambda 2\pi\nu_{\rm rf}\, q[e]}, \quad \frac{\lambda}{\Delta x} = \left(\frac{j_{d0}}{2\pi\nu_{\rm rf}\, q[e]\Delta x}\right)^{1/2}. \tag{5}$$

If $\Delta x > \lambda$ then j_{d0} is corrected and used to compute circuit parameters, among them the dc substrate bias. A similar procedure is followed in the PCMCS to obtain the actual sheath thickness λ, and will be discussed below. This coupling of an analytic sheath model and bulk plasma model for a rf discharge has recently been reported by Nitschke and Graves.[26]

B. PCMCS

At the end of the HPEM electron impact source functions, and time and position dependent electric fields are exported to the PCMCS. The PCMCS also accepts the advective flow field from the HM. The PCMCS launches pseudoparticles representing ions and neutral species during the rf cycle from locations weighted by the electron impact source functions obtained from the HPEM. The trajectories of the pseudoparticles are followed in a time dependent fashion using interpolated electric fields (position and phase). Surface reactions are represented by reactive sticking coefficients. Particle-mesh algorithms are used to represent ion–ion, ion–radical, and radical–radical collisions. In doing so, statistics on the densities of radicals and ions are collected during the flight of the pseudoparticles and transferred to the mesh. The pseudoparticles then collide with the mesh defined densities. A converged solution is obtained by iterating through many flights (or launchings) of pseudoparticles.

Pseudoparticles for each species j are launched in the reactor in accordance with the spatial distribution of the electron impact source functions $S_j(r,z)$ obtained from the HPEM. The number of pseudoparticles of species j launched from a given computational cell centered on (r,z) having volume $V(r,z)$ is

$$N_j(r,z) = N_t \frac{S_j(r,z)V(r,z)W_j(r,z)}{\int[\Sigma_i S_i(r,z)V(r,z)W_i(r,z)]d^3r}, \tag{6}$$

where N_t is the total number of pseudoparticles being launched, the sum in the denominator is over all species being initialized, and W_i is a weighting function. Since the dynamic range of the electron impact source functions can span many orders of magnitude, launching a statistically relevant number of pseudoparticles from each cell is problematic. To address this issue, we weight the number of particles launched from each cell by

$$W_j(r,z) = \frac{\log[S_j(r,z)]}{\log(S_m)}, \tag{7}$$

where S_m is the maximum value of all electron impact source functions. The ith particle of species j launched from cell (r,z) is then "tagged" as representing

$$m_{ij} = \frac{S_j(r,z)V_j(r,z)}{N_j(r,z)} \tag{8}$$

actual particles, with m_{ij} having units of s^{-1}. Some of the source functions from the HPEM are locally negative as a result of processes such as electron–ion recombination, detachment, or multistep ionization. In these cases, the source function is excluded from calculation of the launch weights of pseudoparticles. The loss of these particles are accounted for by collisions with a dummy species which removes particles at the rate specified by $S_i(r,z)$.

The pseudoparticles are launched with velocities

$$\mathbf{v}(r,z) = \mathbf{v}_t + \mathbf{v}_a(r,z), \tag{9}$$

where $\mathbf{v_t}$ is a thermal velocity randomly selected from a Maxwell–Boltzmann distribution having the gas temperature, and $\mathbf{v_a}$ is the local advective velocity obtained from the HM. Statistics on the volumetric densities $N_j(r,z)$ of each species are then obtained by integrating the time each particle spends in a given computational cell:

$$N_j(r,z) = \sum_i \int m_{ij}\delta(r_{ij}-r)\delta(z_{ij}-z)\,dt. \tag{10}$$

When all pseudoparticles are collected or otherwise removed from the simulation, the computational iteration is complete. The species densities derived as described above are used to recalculate collision frequencies, and another "flight" of pseudoparticles are released, constituting the next iterations. Depletion of feedstock gases which may not be tracked using Monte Carlo particles is accounted for by reducing their fluid background densities by the appropriate densities of their daughter species. Back averaging of the iteration-by-iteration derived densities is performed to speed convergence.

Trajectories are advanced by direct integration of the velocities between collisions. For neutral species, the trajecto-

ries are free flight. For ions, accelerations are included as specified by the local electric fields. These fields are obtained by performing a three-dimensional interpolation (r, z, and time during the rf phase) of the electric fields imported from the HPEM. The flight time is determined by

$$\Delta t = \min(\Delta t_r, \Delta t_z, \Delta t_c, \tau), \tag{11}$$

where Δt_r and Δt_z are the times to cross a specified fraction of the computational cell in the r and z directions, Δt_c is the time to the next collision, and τ is a specified fraction of the rf cycle. The time to cross the computational cell is determined by solving the quadratic equation of motion for Δt using the local electric field. The time to the next collision for species j is

$$\Delta t_{\mathrm{col}} = -\left(\sum_k \nu_{j,k} \right)^{-1} \ln(1-r), \tag{12}$$

where $\nu_{j,k}$ is the collision frequency of species j for process k and r is a random number evenly distributed on (0,1). If a particle collides with a surface during a flight (which results in the particle "appearing" in a solid) the point of intersection of the particle with the surface is backcalculated. The particle is then placed at the surface, and the disposition of the particle is determined as described below.

Collision dynamics are accounted for by constructing probability arrays for each species j. These arrays are

$$P_{ij} = \frac{\sum_{m=1}^{i} k_{mj} N'_{mj}}{\sum_{m=1}^{i-\max} k_{mj} N'_{mj}}, \tag{13}$$

where k_{ij} is the effective two-body rate coefficient for the ith heavy particle collision of species j and N'_{ij} is the density of its collision partner. The prime indicates that the maximum density of the collision partner throughout the reactor is used to construct these arrays, thereby implementing a modified null cross section.[20]

When a particle reaches the randomly selected time for a collision, the collision which occurs is determined by selection of another random number r. The collision which occurs satisfies $P_{i-1,j} < r \leqslant P_{i,j}$. Given this choice of collision, the actual occurrence of the reaction is denoted by choice of a third random number r,

$$r \leqslant \frac{N_{ij}(r,z)}{N'_{ij}}, \tag{14}$$

where $N_{ij}(r,z)$ is the actual local density of the collision partner. This technique allows for null collisions to account for transport of the particle between locations having different densities of the collision partner.

A variety of heavy particle collisions are included in the model. If the collision is an identity changing collision (e.g., $Ar^+ + Cl_2 \rightarrow Ar + Cl_2^+$), the characteristics of the particle are changed (i.e., mass, charge), and particles are added or subtracted accordingly. In the case of thermal chemical reactions in the bulk plasma, the velocities of the products are randomly chosen from a Maxwell–Boltzmann distribution having the local gas temperature. In the case of a charge exchange collision, the hot neutral retains the original ion's velocity. The rate coefficients for elastic collisions are calculated using Lennard-Jones parameters to simulate hard sphere collisions. The Lennard-Jones parameters used in the model were obtained from Ref. 27. Since all collision dynamics are on a particle-mesh basis, we do not have vector velocity information on the mesh collision partner. Therefore, in an elastic collision, the mesh defined collision particle is given a velocity which is the sum of a random thermal (Maxwellian) velocity and the local advective velocity. In this way, following a series of collisions, the pseudoparticle "feels" the effects of the advective flow. A similar algorithm was used in a model for remote plasma tools, and is described in Ref. 28.

C. Correction for submesh sheath thickness in the PCMCS

As discussed in Sec. II A, we have employed a semianalytic model in the HPEM to correct for submesh sheath thickness. The effect in the PCMCS of using a mesh limited sheath thickness which exceeds the actual sheath thickness is that the computed transit time of the ions is too large, thereby reducing the width of the IED. We have used the same sheath model in the PCMCS to account for submesh sheath thickness in the following manner. Prior to executing the PCMCS, we delineate the thickness of the sheath by inspecting the electric fields $E(r,z,\phi)$ obtained from the HPEM. If the thickness of the sheath exceeds one computational cell perpendicular to a surface, no correction is applied. In the event the sheath thickness is less than a single cell width, we reduce the width of the cell in the perpendicular direction to be equal to the actual sheath thickness. In order to conserve the voltage drop across the sheath, the electric field in the compressed boundary cell is increased by the factor $\Delta x/\lambda$. This treatment effectively results in having a fixed sheath thickness throughout the rf cycle while the sheath voltage drop oscillates.

D. Surface reactions

Surface reactions are included in the PCMCS using a reactive sticking coefficient r_s which specifies the probability that the pseudoparticle reacts with the surface (and is removed from the gas phase). r_s is a function of the incident species and material which the species strikes. When a particle collides with the surface, a random number is chosen. If $r \leqslant r_s$, a reaction occurs. If the inequality does not hold, the particle is diffusively reflected from the surface with a speed randomly chosen from a Maxwell–Boltzmann distribution having the wall temperature. If the reaction occurs, a second random number is chosen to determine the disposition of the particle in accordance with the surface reaction mechanism.

The particles which are returned to the gas leave from the surface with polar angle based on a modified cosine or Lambertian distribution. The maximum polar angle with which the particle can leave the surface is limited to being less than 60° to restrict scattering at grazing angles to account for surface roughness. In the case of ions, the neutralized particle is also allowed to return to the plasma with a specified fraction of its incident energy, which allows for spectral scattering from the surface.

In the cases discussed here, we use an Ar/Cl_2 chemistry. Other than neutralization of ions and quenching of excited states, the only reaction chemistry on surfaces in the examples we will discuss involves the Cl radical. The reactive sticking coefficient for chlorine on nonwafer surfaces was estimated as $r_s = 0.005$, generating the product Cl_2 which diffusively returns to the plasma. On the wafer, Cl reacts with an average $r_s = 0.05$, generating the etch product $SiCl_2$. The small r_s on the wafer is intended to account for the finite open area of p-Si on the wafer.

E. Etch model

The etch mechanism of Dane and Mantei[23] for a chlorine plasma was used to calculate etch rates at the wafer and production rates of gaseous etch products. The etch model is based on the surface reaction scheme

$$\mathrm{Cl(g)+Si(s)\rightarrow SiCl(a)}, \tag{15a}$$

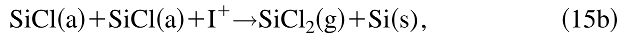

$$\mathrm{SiCl(a)+SiCl(a)+I^{+}\rightarrow SiCl_2(g)+Si(s)}, \tag{15b}$$

where SiCl(a) represents Cl passivation of Si on the surface, and I^+ represents activation energy delivered to the surface by ions. The resulting etch rate is

$$\mathrm{ER} = \left(\frac{1}{\alpha \Gamma_{\mathrm{Cl}}} + \frac{1}{\beta [J_i V_s - (JV)_{\mathrm{th}}]} \right)^{-1}, \tag{16}$$

where α and β are semiempirical parameters, Γ_{Cl} is the Cl radical flux to the wafer, $(JV)_{\mathrm{th}}$ is a threshold power flux to the wafer for the onset of etching, and $J_i V_s$ is the actual power flux. Dane and Mantei approximated the power flux as the product of ion current into the sheath and sheath potential. They derived values for the parameters based on etching of p-Si in Cl_2 ECR plasmas. They obtained α=2300 $\text{Å}\,\text{min}^{-1}\,\text{mTorr}^{-1/2}$, β=23 $\text{Å}\,\text{min}^{-1}\,\text{mW}^{-1}\,\text{cm}^2$, and $(JV)_{\mathrm{th}}$=85 mW cm^{-2}. Since Dane and Mantei were not able to directly measure the chlorine radical flux, they derived a semiempirical relationship for the flux in which $\Gamma_{\mathrm{Cl}} \propto \sqrt{P_{\mathrm{Cl}_2}}$, where P is the partial pressure of Cl_2.

In applying this etch mechanism in our model, we have the benefit of being able to directly calculate Γ_{Cl} and the power flux to the wafer. In doing so, we must rederive the parameter α in terms of a true particle flux. This parameter was first converted to units of ($\text{Å}\,\text{min}^{-1}\,\text{cm}^2\,\text{s}$) by estimating the value of Γ_{Cl} in the Dane and Mantei experiments. Using an estimated 50% dissociation of Cl_2 at 1 mTorr and a gas temperature of 600 K, the thermal flux of Cl to the wafer is $\approx 3.5\times 10^{17}$ $\text{cm}^{-2}\,\text{s}^{-1}$. The renormalized parameter is then $\alpha = 6.54\times 10^{-15}$ ($\text{Å}\,\text{min}^{-1}\,\text{cm}^2\,\text{s}$). One should consider this estimate as an upper limit, since it does not account for spatial nonuniformity of the Cl flux and the effects of macroloading at the wafer.

Γ_{Cl} was obtained from the model by summing the weightings of all Cl and Cl* pseudoparticles as a function of position on the wafer, and dividing by surface area of the computational cell. Since the weightings of the particles have units of s^{-1}, this sum provides an atom flux. The power flux was obtained by summing the products of the weightings and kinetic energy of all ions incident onto the wafer, and normalizing by the area.

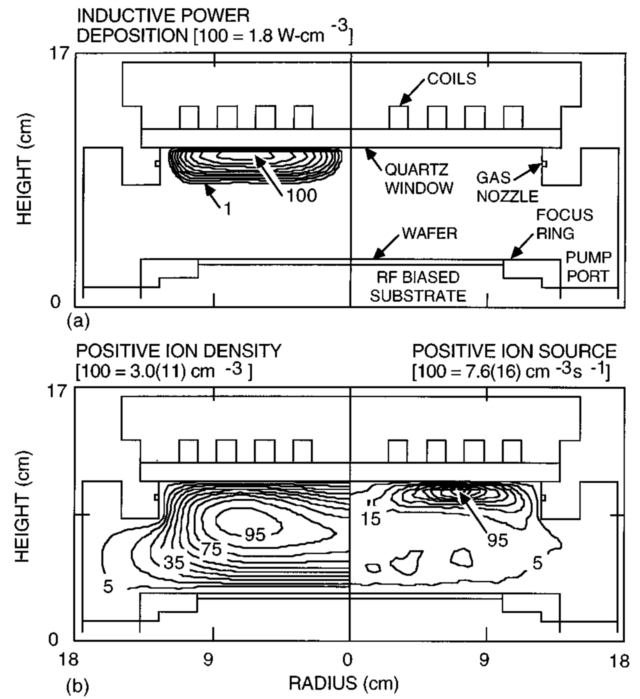

FIG. 1. Typical plasma properties in an ICP etching reactor obtained with the hybrid plasma equipment model. (a) Reactor schematic and inductively coupled power deposition, (b) total positive ion density (sum of Ar^+, Cl^+, Cl_2^+), and positive ion sources by electron impact. The gas mixture is Ar/Cl_2=70/30 at 10 mTorr, 500 W of inductively coupled power, and 100 V bias applied to the substrate. The annular power deposition produces an off-axis maximum in the positive ion density and source. (The contour labels are percentage of the maximum value shown at the top of each panel).

III. ION ENERGY DISTRIBUTIONS IN ICP REACTORS

In this section, we will discuss spatially dependent IEDs incident on the wafer in an inductively coupled plasma etching reactor. The geometry we used resembles the Lam Research Corporation 9400 transformer coupled plasma (TCP) etching tool, and is shown in Fig. 1. The plasma is generated by the 13.56 MHz inductively coupled electric field produced by a flat spiral coil on top of a quartz window above and parallel to the substrate. The 20-cm-diam wafer sits on an rf biased substrate, also at 13.56 MHz, 180° out of phase to the coil. The wafer is surrounded by an alumina focus ring. Gas is injected through inwardly pointing nozzles at a flow rate of 80 sccm and pumped out at the base of the reactor. The gas mixtures we have investigated are Ar/Cl_2=70/30 at pressures of 5–20 mTorr. The rate coefficients for gas phase neutral chemical and ion–molecule reactions used in the model are the same as listed in Ref. 20. In addition to those reactions, we include elastic collisions between all species, whose rate coefficients are computed using Lennard-Jones parameters in the manner described above. The inductively coupled power ranges from 150 to 1000 W, and the substrate biases range from 0 to 150 V (amplitude).

A. Base case

The base case for our study uses the Ar/Cl_2 gas mixture at 10 mTorr, 500 W ICP power with an rf bias of 100 V

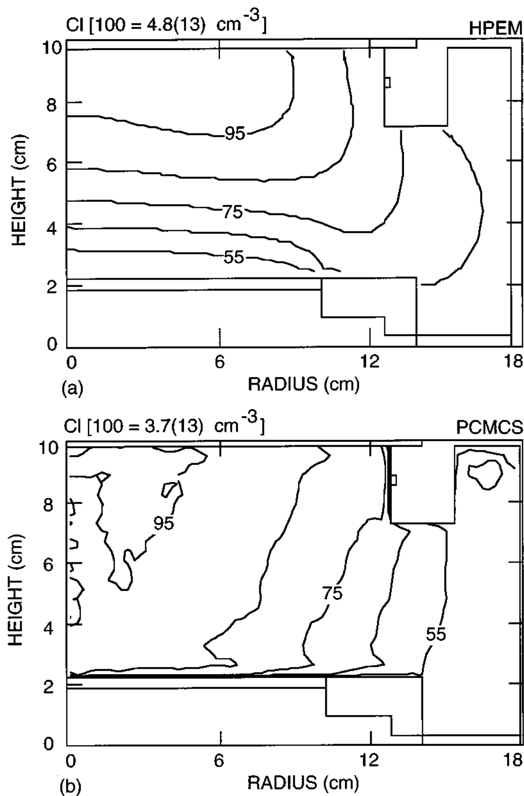

FIG. 2. Cl atom densities for the conditions of Fig. 1 (Ar/Cl_2=70/30, 10 mTorr, 500 W, 100 V bias) obtained from the (a) hybrid plasma equipment model and (b) plasma chemistry Monte Carlo simulation. Although peak densities and profiles are similar, long mean free path transport better represented by the PCMCS reduces density gradients near the wafer.

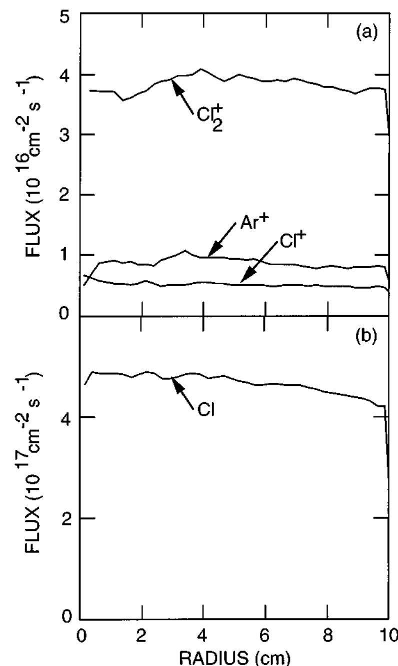

FIG. 3. Fluxes to the wafer obtained with the PCMCS for the conditions of Fig. 1 (Ar/Cl_2=70/30, 10 mTorr, 500 W, 100 V bias) as a function of radius. (a) Fluxes of positive ions (Ar^+, Cl^+, Cl_2^+) and (b) neutral Cl atoms. In spite of the nonuniform source of ions, transport is sufficiently collisional to produce uniform ion fluxes to the wafer. A low sticking coefficient for Cl on nonwafer surfaces contributes to its uniform flux.

amplitude on the substrate. The power deposition, positive ion density (sum of Ar^+, Cl^+, and Cl_2^+), and the positive ion source obtained from the HPEM are shown in Fig. 1. The calculated dc bias on the substrate is -31 V. The resistive inductively coupled power deposition has a maximum of 1.8 W/cm^3 and is located 1–2 cm below the quartz window due to the finite skin depth of the inductively coupled field into the plasma. Due to the long mean free path of electrons at 10 mTorr, the electron impact source for Cl_2^+ is more extended than that for power deposition.

The Cl atom densities predicted by the HPEM and PCMCS are shown in Fig. 2. The magnitudes and shapes of the densities obtained using the two methods are similar except near the wafer. The Cl atom gradient is steeper near the wafer (a sink for Cl atoms) in the results from the HPEM which uses continuum equations. The PCMCS portrays the Cl atom density near the wafer with more nearly a jump condition. This is a consequence of the Monte Carlo techniques in the PCMCS being able to resolve long mean free path transport.

The fluxes to the wafer for positive ions and Cl atoms obtained with the PCMCS are shown in Fig. 3. Even though the ions are not generated uniformly, the substrate-to-source distance is sufficiently large that diffusion smoothes the ion flux profile to the wafer. There is a slight maximum at half the radius which mirrors the source function. The flux is dominated by Cl_2^+, due to the lower threshold for ionization of Cl_2 compared to Ar, and the fact that Cl_2^+ is produced in the nonsymmetric charge exchange of Cl_2 with Ar^+ and Cl^+. The flux of Cl is also fairly uniform. The transport of Cl radicals is diffusion dominated and, when combined with a low sticking coefficient at the walls, leads to high radial uniformity.

The radially averaged energy distributions of neutral particles striking the substrate are shown in Fig. 4. The neutrals generally impact the wafer with a nearly Maxwellian velocity distribution with temperature of 600–700 K. The heating is largely due to charge exchange reactions which also forms a high energy tail. The most important process in this regard is the symmetric charge exchange for Ar, since the density of the feedstock argon is the largest and its cross section for charge exchange is large. This process generates hot Ar atoms with broad energy distributions at the wafer reaching as high as 20–30 eV and with fluxes of 3×10^{17} cm^{-2} s^{-1}, as shown in Fig. 4. This corresponds to power fluxes to the wafer of $\sim$20 mW/cm^2. Although these power fluxes are not included in our calculations of etching rates, they are large enough to contribute to the activation energy for etching if we consider hot atom and ion impact energy as being equivalent.

The IEDs averaged over the wafer for Ar^+, Cl_2^+, and Cl^+ are shown in Fig. 5 for a 100 V (amplitude) bias. The IEDs clearly show the characteristic bimodal distribution resulting from short ion transit times (with respect to the rf period) usually associated with lower frequency operation in RIE discharges. The short ion transit times result from the thin

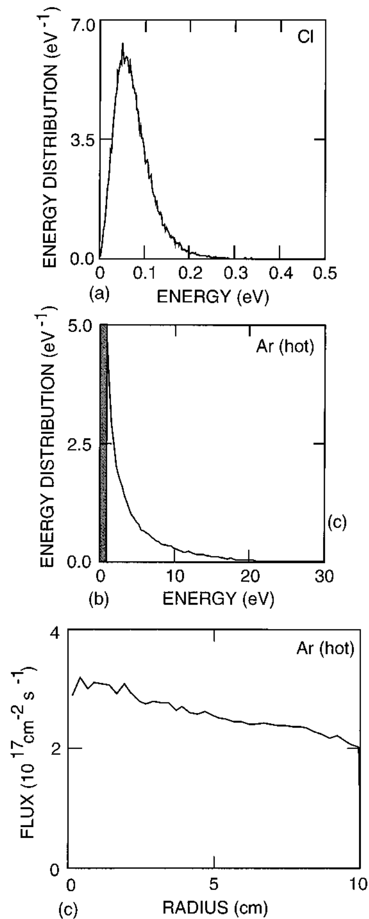

FIG. 4. Energy distributions and fluxes for neutral particles striking the wafer predicted by the PCMCS. (a) Cl atoms, (b) hot Ar atoms, and (c) hot Ar flux. Hot atoms are defined as having energies >0.5 eV. The average Cl temperature striking the wafer is ≈600 K. Hot Ar atoms produced by charge exchange have a tail to 20 eV, and a power flux of 10s mW cm^{-2}.

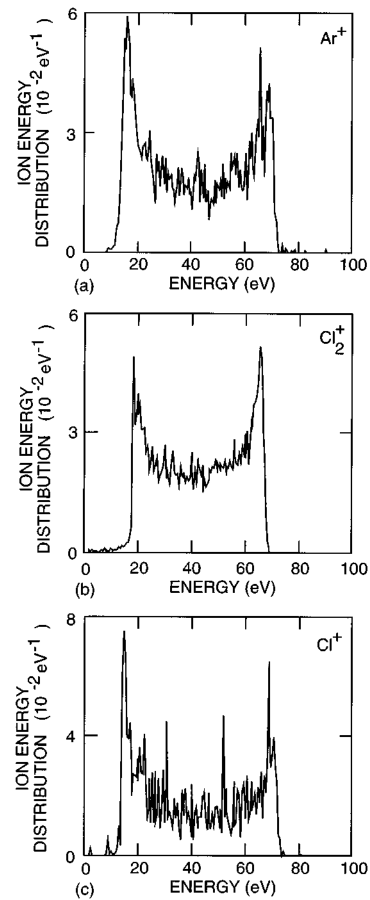

FIG. 5. Ion energy distributions (IEDs) averaged over the wafer for an ICP power deposition of 500 W, and rf bias of 100 V. (a) Ar^+, (b) Cl_2^+, and (c) Cl^+. The sheath is sufficiently thin that the ions respond to the instantaneous bias. The lighter Cl^+ and Ar^+ IEDs have larger widths.

sheaths for these conditions, ≈0.05 cm, produced by the high plasma density. For this sheath thickness the transit time for Ar^+ is ⩽30 ns, which is shorter than the rf period 13.56 MHz (74 ns). This allows the ions to "sense" the instantaneous sheath potential. The Cl^+ ion, having a mass comparable to Ar^+, has a similar IED. In spite of the Ar^+ having a large rate of charge exchange, there is no evidence for such collisions in the IED. The thin sheath and low gas pressure results in the sheath being nearly collisionless. Since Cl_2^+ is almost twice as massive as Ar^+, its transit time is longer, ≈40 ns resulting in the Cl_2^+ ion "sensing" a more averaged sheath potential, producing an IED having a somewhat narrower width.

Using the standard four-turn coil (see Fig. 1), the electron density at the wafer and current densities to the wafer are fairly uniform as a function of radius, as shown in Fig. 6. (The electron density shown in Fig. 6 is the cycle averaged value at the sheath side of the presheath.) There is a small reduction in the electron density and the conduction current density at large radius, while the displacement current increases slightly. Since the width of the sheath is proportional to the displacement current and inversely proportional to the electron density, the sheath thickness increases at the outer edge of the wafer from 0.45 to 0.50 mm. The thickening of the sheath over the outer few cm radius of the wafer produces a small narrowing in the Cl_2^+ IED of <5 eV at those locations, but the IED is otherwise uniform as a function of radius.

To demonstrate the possibility that the shape of the IED can be a function of radius, we ran the HPEM while powering only the inner two coils. This results in power deposition and ion sources being located near the axis.[20] The electron density adjacent to the wafer and the current density to the wafer are peaked at the center of the wafer, decreasing by more than a factor of 2 at the edge of the wafer, as shown in Fig. 6. The sheath width has a commensurate increase near the edge of the wafer. These conditions cause the Cl_2^+ IED to become noticeably narrower near the edge of the wafer [shown in Fig. 6(d)].

The average angle of incidence and energy of ions are essentially constant as a function of position on the wafer with the four turn coil. The average angle of incidence of Cl_2^+ is ≈8° for an rf bias of 100 V with an average impact energy of 40 eV. This corresponds to ions entering the sheath with temperatures of 0.5–1 eV, which agrees with the experiments of O'Neill *et al.*[5] For the unbiased substrate, the aver-

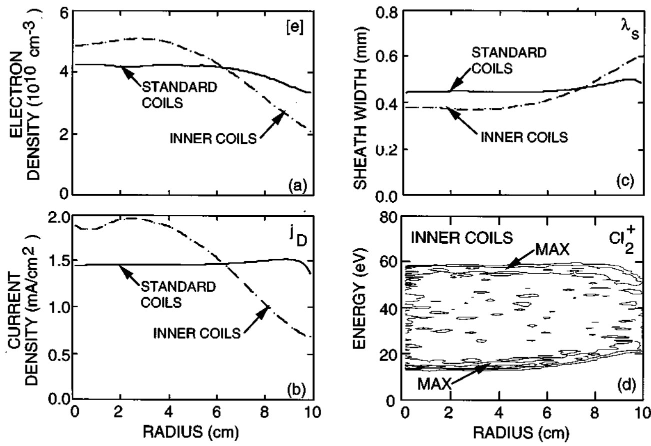

FIG. 6. Plasma properties as a function of radius. (a) Cycle averaged electron density at the edge of the sheath, (b) displacement current density to the wafer, (c) sheath width, and (d) IED for Cl_2^+. Results are shown for the standard four-turn coil (solid line) and when only the two inner coils are powered (dashed lines). The IED is only shown for the two-turn inner coil configuration. The reduced plasma density and thicker sheath at the edge of the wafer with the two-turn inner coil configuration produces a narrow IED.

age incident angle is 29°, since the potential drop across the sheath is due only to the floating potential, producing ions with an average impact energy of 10 eV, with an ion temperature entering the sheath of 0.5–1 eV. The high temperature of the ions results largely from acceleration through the presheath. These results agree well with both direct measurements of the IED in unbiased systems, and with the implied temperature of ions required to account for etch profiles.[10–12]

B. IEDs as a function of ICP power and rf bias

IEDs for Cl_2^+ are shown in Fig. 7 for rf biases (amplitudes) of 50, 100, and 150 V, and an ICP power of 500 W. The dc self-biases are -13, -31, and -37 V, respectively. The widths [full width at half-maximum (FWHM) in energy] of these distributions are shown in Fig. 8. There is an expected increase in average ion energy from 20 eV for the 50 V bias case to 70 eV for the 150 V bias case. The increase in ion energy results not only from the increase in the amplitude of the rf bias but also from the increase in the dc bias. The widths of the IEDs also increase with increasing bias amplitude, a consequence of the short transit time of ions which allow the ions to nearly track the instantaneous sheath potential. This is somewhat counterintuitive since the sheath thickness increases nearly linearly with increasing bias, as shown in Fig. 9. However, since the transit time of the ion through the sheath scales as $\tau_t \sim (\lambda^2/V)^{1/2}$, the bimodal character of the IED is retained at larger biases. In general, the widths of the distributions for Cl_2^+ are $\approx$50% of the bias amplitude, since the ion transit time is $\approx$50% of the bias cycle time. The low energy peaks of the IEDs decrease relative to the high energy peak as the bias increases. This trend indicates that the sheath appears more resistive at the lower bias. The ion conduction current through the sheath is a function primarily of plasma density, which is a weak function of bias voltage,

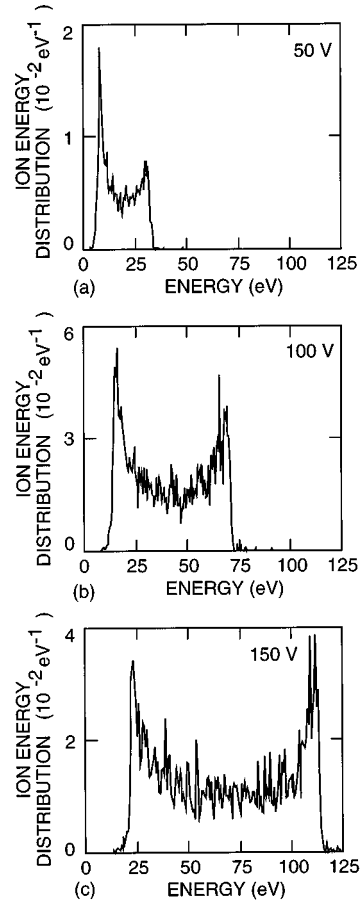

FIG. 7. IEDs for Cl_2^+ averaged over the wafer for an ICP power deposition of 500 W and different rf biases. (a) 50, (b) 100, and (c) 150 V. The IEDs are broader in energy with increasing bias. The dc bias also becomes more negative.

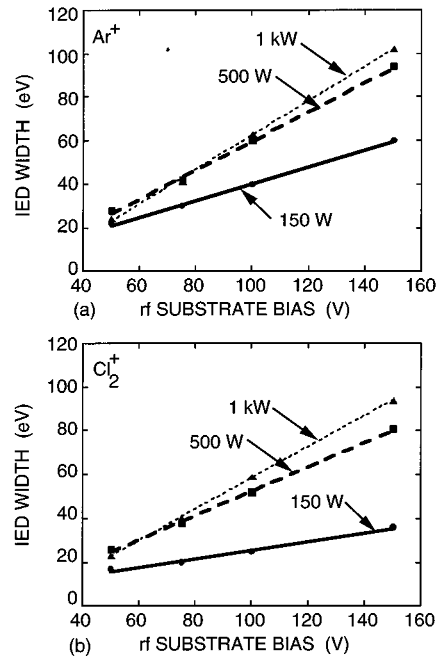

FIG. 8. Energy width of the IED (FWHM) as a function of rf substrate bias for different ICP powers. (a) Ar^+ and (b) Cl_2^+. The width of the IED increases with increasing rf bias due to the larger sheath amplitude, and increases with increasing ICP power due to the decreasing sheath thickness. The heavier Cl_2^+ has a narrower IED.

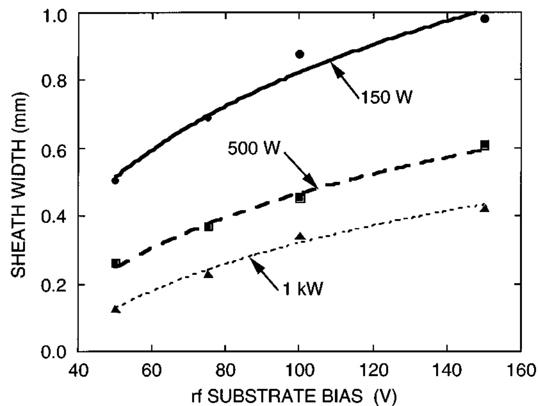

FIG. 9. Sheath width as a function of rf substrate bias for different ICP powers. The sheath width increases with increasing rf bias and decreasing ICP power.

while the displacement current increases with increasing bias voltage. Therefore, one should expect a less resistive sheath at higher biases.

Over the ranges of power investigated (150 W to 1 kW) the plasma density increases nearly linearly with the ICP power. As a result, the sheath thickness decreases with increasing ICP power, as shown in Fig. 9. As a consequence of the reduced sheath width, the ion transit time decreases with increasing ICP power, resulting in a corresponding increase in the widths of the IEDs. This trend is shown in Fig. 10 where IEDs for Ar^+ and Cl_2^+ are plotted as a function of rf bias for ICP powers of 150 W and 1 kW. The FWHM of IEDs for various ICP powers and rf biases are summarized in Fig. 8. The widths of the IEDs increase with increasing ICP power and increasing rf bias. Since the Cl_2^+ is the heaviest ion and its transit time is longer than that of the Ar^+, the decrease in sheath thickness from 0.88 mm at 150 W to 0.34 mm at 1 kW has a much greater effect on its IED. At 150 W, the width of the Cl_2^+ IED is 25 eV, which corresponds to a transit time of 80%–85% of the rf cycle. The width of the Ar^+ IED is 40 eV, having a sheath transit time of 60%–65% of the rf cycle. At 1 kW, the Cl_2^+ and Ar^+ IED widths have increased to 57 and 65 eV, respectively, a consequence of the transit times for both ions dropping to only 20%–30% of the rf cycle. At low powers, where the sheath is thicker, the width of the Cl_2^+ IED is little affected by increasing the rf bias amplitude. At higher powers, where the sheath has thinned, the IEDs of both Ar^+ and Cl_2^+ increase as the bias amplitude is increased.

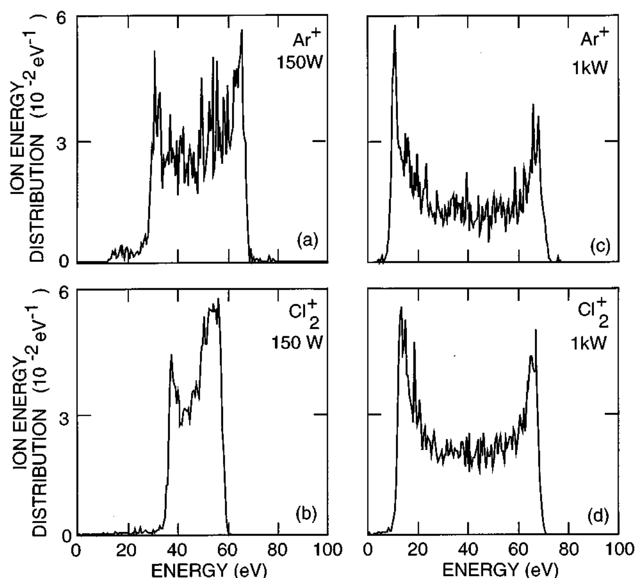

FIG. 10. IEDs averaged over the wafer for different ICP power with 100 V of rf bias: (a) Ar^+ and (b) Cl_2^+ for 150 W ICP power; (c) Ar^+ and (d) Cl_2^+ for 1 kW ICP power. Low ICP power results in thick sheaths which, for the heavier ions, results in the ion transit time being many rf cycles. This produces a narrow IED. At high power, the transit time is on the order of one rf cycle.

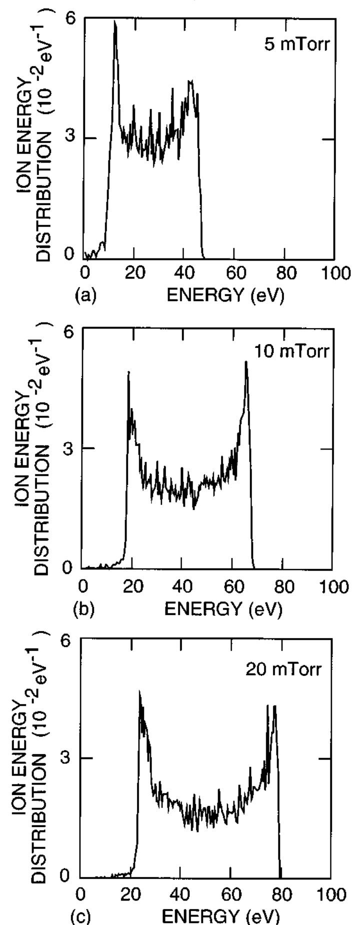

FIG. 11. IED for Cl_2^+ for different pressures (500 W ICP, 100 V rf bias). (a) 5, (b) 10, and (c) 20 mTorr. For these conditions, the plasma density increases with increasing pressure, thereby decreasing the sheath width. Even at 20 mTorr, the sheath is essentially collisionless.

In spite of the broadening of the IEDs with increasing ICP power, we observe a decrease in the average ion energy at the wafer of ≈5 eV when increasing the ICP power from 150 W to 1 kW. The decrease in average ion energy is attributed to a decrease in dc bias (becoming less negative) with increasing ICP power. This trend agrees with the experiments of Fusakawa *et al.*[29] who observed less negative dc biases with increasing ICP power.

The IEDs for Cl_2^+ are shown in Fig. 11 for gas pressures of 5, 10, and 20 mTorr. The IED increases in width and increases in average energy with increasing gas pressure. Over this range of power deposition, the sheath is essentially collisionless. The change in the character of the IED is therefore attributable to electrical properties. In going from 5 to 20 mTorr, the dc bias becomes more negative, which increases the average energy of the IED. At higher gas pressures, the plasma becomes more confined. In this particular geometry, a more confined plasma appears more asymmetric with respect to the capacitively coupled plasma, thereby increasing the dc bias. Also over this range of pressures, the plasma density decreases with decreasing pressure, thereby increasing the width of the sheath and narrowing the IED.

C. Ion and neutral fluxes

Ion and radical fluxes as a function of radius on the wafer are shown in Fig. 12(a) as a function of rf bias for an ICP power of 500 W and gas pressure of 10 mTorr. For these conditions, Cl_2^+ has the highest flux to the substrate, followed by Ar^+ and Cl^+. The rf bias has little effect on the magnitude of fluxes to the wafer for either the neutral radicals, in this case Cl, or for the ions. The ratios of the ion fluxes also change little. The small change in magnitude of the fluxes with rf bias confirms the fact that the rf bias is contributing little to the total rate of ionization in the plasma, and serves primarily to accelerate ions. There is, however, a small improvement in the uniformity of the ion flux at the higher rf bias as shown in Fig. 13. This improvement is due to improved radial uniformity of the ion density in the reactor resulting from a flattening of the time-averaged plasma potential.

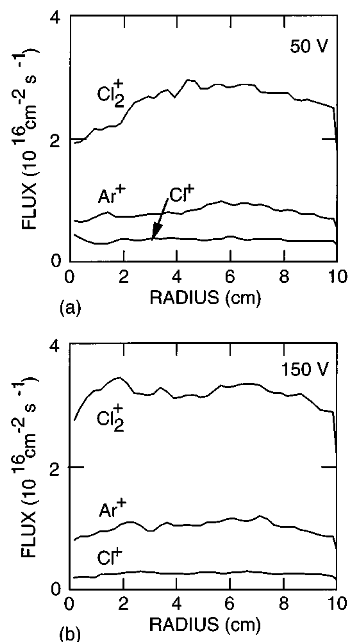

FIG. 13. Fluxes of Ar^+, Cl^+, and Cl_2^+ as a function of radius for rf biases of (a) 50 and (b) 150 V. The larger rf bias produces a more favorable distribution of plasma potential, resulting in a more uniform ion flux to the wafer.

As previously discussed, over the ranges investigated, the plasma density is nearly linearly proportional to the power deposition at constant pressure. Therefore, one should also expect nearly linear increases in the fluxes to the wafer with increasing power. This trend is also shown in Fig. 12(b), where the Cl and positive ion fluxes are plotted as a function of ICP power for a rf bias of 100 V. There is a small decrease in the uniformity of the flux at higher power deposition due to more localized power deposition and sourcing of the ions which occurs at higher conductivities and thinner inductive skin depths. The composition of the ion fluxes are a more sensitive function of gas pressure as shown in Fig. 14. The fractional Cl_2^+ flux increases with increasing pressure, while

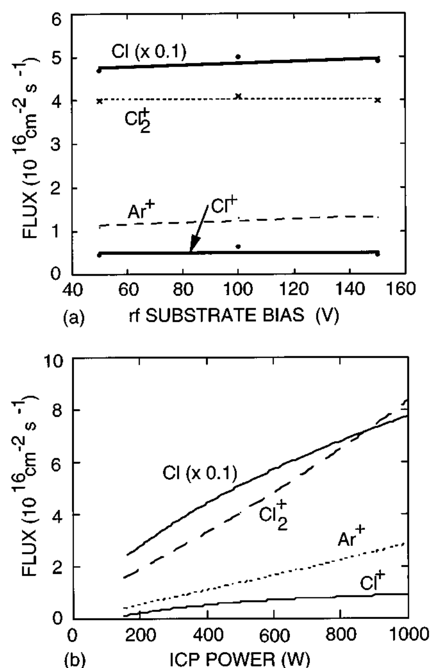

FIG. 12. Fluxes of Cl, Ar^+, Cl^+, and Cl_2^+ to the wafer as a function of radius. (a) Fluxes at 500 W as a function of rf substrate bias. (b) Fluxes at a rf bias of 100 V as a function of ICP power. The magnitudes of the fluxes are insensitive to the rf bias, and are controlled by the ICP power.

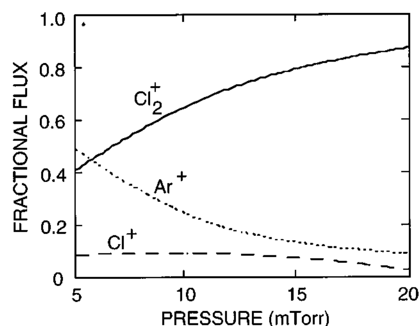

FIG. 14. Fractional fluxes of Ar^+, Cl^+, and Cl_2^+ averaged over the wafer as a function of gas pressure. At higher gas pressures, increasing rates of charge exchange favor the Cl_2^+ ion flux.

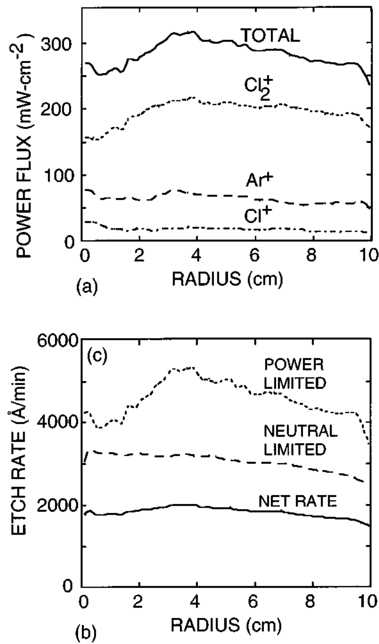

FIG. 15. Poly-silicon etch characteristics. (a) Ion power flux to the wafer as a function of position due to the separate positive ions and total power. (b) Etch rates as a function of radius as implied by power limiting, neutral limiting, and the total rate. The high frequency variation in the power flux is numerical noise from the Monte Carlo simulation.

the fractional Ar^+ and Cl^+ fluxes decrease. This trend results from the fact that Ar^+ charge exchanges with Cl and Cl_2, producing Cl_2^+ in the latter reaction. Cl^+ charge exchanges with Cl_2, also producing Cl_2^+. Cl_2^+, however, does not charge exchange with either Ar or Cl. The increase in pressure therefore efficiently converts Ar^+ and Cl^- to Cl_2^+.

IV. PREDICTED ETCHING RATES

The mechanism of Dane and Mantei for chlorine etching of poly-Si was used to predict etching rates for the Ar/Cl_2 ICP discharges. The predicted radical and ion power fluxes incident on the wafer as a function of position for the standard case [Ar/Cl_2=70/30, 10 mTorr, ICP power=500 W, rf bias (amplitude)=100 V] are shown in Fig. 15. The Cl radical flux is uniform to within 10% over the 10 cm radius of the wafer, and maximum at the center of the reactor. The ion power flux (which shows numerical noise) has a local maximum at midradius as a consequence of the nonuniform power deposition. The Cl_2^+ ion contributes approximately 60% of the power flux, in proportion to its total molecular flux. The predicted power flux limited etch rate (i.e., the etch rate which one would predict with infinite Cl flux) is ≈5000 Å/min, and reflects the nonuniform power flux to the wafer. The neutral limited etch rate (i.e., the etch rate which one would predict with an infinite power flux) is ≈3000 Å/min and is uniform as a function of radius. The combined etch rate has an average value of 1850 Å/min. It is uniform to within 10% over 90% of the radius of the wafer, reflecting the uniformity of the Cl atom flux with some small enhancement due to the local maximum in the ion power flux. This etch rate corresponds to a flux rate of $SiCl_2$ from the surface

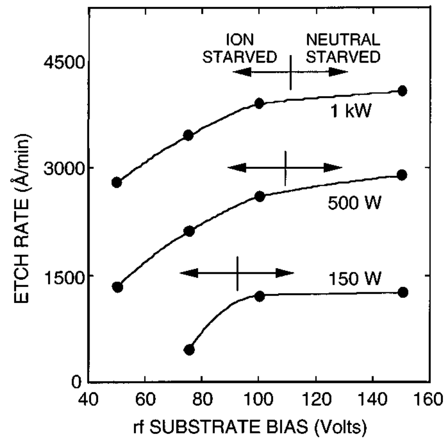

FIG. 16. Radially averaged etch rates as a function of rf bias for various ICP powers. At low rf biases, the ion power flux is low relative to the neutral flux, and the system is ion starved. At high rf biases, the etch rate is limited by the availability of Cl atoms, and is in the neutral starved regime.

of 1.5×10^{16} $cm^{-2}\,s^{-1}$. For an ion flux of $\approx7\times10^{16}$ $cm^{-2}\,s^{-1}$, the ratio of ion impacts to etched $SiCl_2$ is 4–5. This value compares well to the results of surface laser desorption studies,[30] as well as the results of Dane and Mantei.[23]

By increasing the rf bias amplitude applied to the substrate, the power flux of ions can be proportionally increased without significantly changing the magnitude of either the ion or Cl atom flux. This increase in power flux should, in principle, increase the etch rate at lower rf biases where the etch rate is ion power flux limited, but not at high rf biases where the etch rate is neutral flux limited. Predicted etch rates as a function of rf bias (amplitude) for ICP powers of 150, 500, and 1000 W are shown in Fig. 16. At low rf biases, the ion power flux is near the threshold value of 85 mW/cm^2. Increasing the rf bias increases the power flux, and so increases the etch rate (the "ion starved" regime). At larger biases where the ion power flux greatly exceeds the threshold value, increasing the power flux at best yields a moderate increase in etch rate. The etch rate is then limited by the availability of Cl atoms (the "neutral starved" regime) and the etch rate approaches a constant value. The etch rates at low ICP power and low rf bias may be underestimated due to lack of a purely thermal component in the etch model as implied by there being a threshold ion power for etching.

V. CONCLUDING REMARKS

A Plasma Chemistry-Monte Carlo model has been developed to investigate the angular and energy distributions, and fluxes of radicals and ions incident on the wafer in high plasma density, low gas pressure inductively coupled plasma reactors. Over the range of ICP powers (150 W to 1 kW) and rf biases [0–150 V (amplitude), 13.56 MHz] investigated, the sheath thickness has a significant effect on the shape of the IEDs at the wafer since ion transit times are commensurate with the rf period. For high ICP power (500 W–1 kW), the sheath is sufficiently thin that the IED has a bimodal

shape typically associated with low frequency operation of low plasma density RIE discharges. For lower powers (150 W) the sheath is thicker. The IEDs are narrower for the same rf bias and arrive at the substrate with the average sheath potential. One of the motivations for ICP reactors is to give separate control of the ion flux and ion power to the wafer. To first order, this control is achieved. The ICP power controls the ion flux to the substrate and, for a given ion flux, the rf bias determines the ion power flux. However at the intermediate powers investigated here, the width of the IED is inversely proportional to the width of the sheath which is in turn inversely proportional to plasmas density and ICP power. The ion flux and ion energy distribution cannot therefore be absolutely independently controlled. There is, however, many combinations of ICP power and rf bias which will provide the desired combinations of ion flux and ion energy characteristics.

The uniformity of poly-Si wafer etching as well as the effects of power, pressure, and bias were investigated using the Dane and Mantei[23] etch mechanism. For the range of powers and biases investigated, high etch rates which were obtained with large rf biases were in the neutral starved regime. Increases in substrate bias beyond 50 to 80 V have little effect on etch rate, especially at higher power. These trends follow those found experimentally by Dane and Mantei for ECR etch tools.[23]

ACKNOWLEDGMENTS

The authors would like to thank Professor Tom Mantei for discussions on the topic of this article. This work was supported by the Semiconductor Research Corporation, the National Science Foundation Grant Nos. (ECS94-04133, CTS94-12565), LAM Research Corp., Sandia National Laboratory/Sematech, and the University of Wisconsin Engineering Research Center for Plasma Aided Manufacturing.

[1] J. Hopwood, Plasma Sources Sci. Technol. **1**, 109 (1992).
[2] J. Keller, M. S. Barnes, and J. C. Forster, 42nd Gaseous Electronics Conference, Urbana, IL, 1990 (unpublished), paper NA-5.
[3] J. H. Keller, J. C. Forster, and M. S. Barnes, J. Vac. Sci. Technol. A **11**, 2487 (1993).
[4] M. S. Barnes, J. C. Forster, and J. H. Keller, Appl. Phys. Lett. **62**, 2622 (1993).
[5] J. A. O'Neill, M. S. Barnes, and J. H. Keller, J. Appl. Phys. **73**, 1621 (1993).
[6] R. Patrick, R. Schoenborn, and H. Toda, J. Vac. Sci. Technol. A **11**, 1296 (1993).
[7] J. B. Carter, J. P. Holland, E. Peltzer, B. Richardson, E. Bogle, H. T. Nguyen, Y. Melaku, D. Gates, and M. Ben-Dor, J. Vac. Sci. Technol. B **11**, 1301 (1993).
[8] Y. Ra, S. G. Bradley, and C.-H. Chen, J. Vac. Sci. Technol. A **12**, 1328 (1994).
[9] D. F. Beale, A. E. Wendt, and L. J. Mahoney, J. Vac. Sci. Technol. A **12**, 2775 (1994).
[10] J. Hopwood, Appl. Phys. Lett. **62**, 940 (1993).
[11] U. Kortshagen, Plasma Sci. Sources Technol. **4**, 172 (1995).
[12] J. Zheng, R. P. Brinkman, and J. P. McVittie, J. Vac. Sci. Technol. A **13**, 859 (1995).
[13] J. Caughman, Proceedings of the 41st National Symposium of the American Vacuum Society, Denver, CO, October 1994 (unpublished), paper PS-MoP5.
[14] A. Manenschijn and W. J. Goedheer, J. Appl. Phys. **69**, 2923 (1991).
[15] M. J. Kushner, J. Appl. Phys. **58**, 4024 (1985).
[16] B. E. Thompson, H. H. Sawin, and D. A. Fisher, J. Appl. Phys. **63**, 2241 (1988).
[17] J. Liu, G. L. Huppert, and H. H. Sawin, J. Appl. Phys. **68**, 3916 (1990).
[18] S. G. Ingram and N. St. J. Braithwaite, J. Phys. D **21**, 1496 (1988).
[19] A. D. Kuypers and H. J. Hopman, J. Appl. Phys. **67**, 1235 (1990).
[20] P. L. G. Ventzek, M. Grapperhaus, and M. J. Kushner, J. Vac. Sci. Technol. B **12**, 3118 (1994).
[21] R. A. Stewart, P. Vitello, and D. B. Graves, J. Vac. Sci. Technol. B **12**, 478 (1994).
[22] M. A. Liebermann, Trans. Plasma Sci. **17**, 338 (1989).
[23] D. Dane and T. D. Mantei, Appl. Phys. Lett. **65**, 478 (1994).
[24] A. Manenschijn, G. C. A. M. Janssen, E. van der Drift, and S. Radelaar, J. Appl. Phys. **69**, 1253 (1991).
[25] A. Metze, D. W. Ernie, and H. J. Oskam, J. Appl. Phys. **60**, 3081 (1986).
[26] R. A. Sveha, NASA Technical Report No. R-132 (1962).
[27] T. E. Nitschke and D. B. Graves, Trans. Plasma Sci. **23**, 717 (1995).
[28] M. J. Hartig and M. J. Kushner, Appl. Phys. Lett. **62**, 1594 (1993).
[29] T. Fukasawa, T. Nouda, A. Nakamura, H. Shindo, and Y. Horiike, Jpn. J. Appl. Phys. **32**, 6076 (1993).
[30] C. C. Cheng, K. V. Guinn, V. M. Donnelly, and I. P. Herman, J. Vac. Sci. Technol. A **12**, 2630 (1994).